



Near- and far-field hydrodynamic interaction of two chiral squirmersRuma Maity  and P. S. Burada **Department of Physics, Indian Institute of Technology Kharagpur, Kharagpur 721302, India*

(Received 8 April 2022; accepted 28 October 2022; published 22 November 2022)

Hydrodynamic interaction strongly influences the collective behavior of microswimmers. With this work, we study the behavior of two hydrodynamically interacting self-propelled chiral swimmers in the low Reynolds number regime, considering both the near- and far-field interactions. We use the chiral squirmer model [see Burada *et al.*, *Phys. Rev. E* **105**, 024603 (2022)], a spherically shaped body with nonaxisymmetric surface slip velocity, which generalizes the well-known squirmer model. The previous work was restricted only to the case, while the far-field hydrodynamic interaction was influential among the swimmers. It did not approach the scenario while both the swimmers are very close and lubrication effects become dominant. We calculate the lubrication force between the swimmers when they are very close. By varying the slip coefficients and the initial configuration of the swimmers, we investigate their hydrodynamic behavior. In the presence of lubrication force, the swimmers either repel each other or exhibit bounded motion where the distance between the swimmers alters periodically. We identify the possible behaviors exhibited by the chiral squirmers, such as monotonic divergence, divergence, and bounded, as was found in the previous study. However, in the current study, we observe that both the monotonic convergence and the convergence states are converted into divergence states due to the arising lubrication effects. The lubrication force favors the bounded motion in some parameter regimes. This study helps to understand the collective behavior of dense suspension of ciliated microorganisms and artificial swimmers.

DOI: [10.1103/PhysRevE.106.054613](https://doi.org/10.1103/PhysRevE.106.054613)**I. INTRODUCTION**

The swimming behavior of microorganisms differs from that of the macro world [1]. In the former case, viscous forces dominate over the inertia of the body. It belongs to the low Reynolds number swimming [1,2]. Different microorganisms employ various propulsion mechanisms, e.g., *Escherichia coli* uses a run and tumble mechanism to propel in a fluid [3]; ciliated microorganisms swim with the help of the metachronal waves generated by the synchronous beating of cilia [4,5], and sperm cells move with the flagella attached to its body [6]. To understand the propulsion mechanism of microswimmers, various models are available in the literature [4–9]. Though the microorganisms are smaller in size, collectively, they can influence the climate and human life in various ways. For example, massive plankton blooms in the ocean, harmful red tides along the coastline, bioconvection [10], nutrient uptake [11], active turbulence [12], and they may even influence the viscosity of the surrounding medium in which they swim [13,14]. In the past, the suspension of microswimmers was studied using a continuum model [15–18], which works well for dilute suspensions only and is generally not applicable for larger cell concentrations. For a denser system, near-field interactions are vital. The hydrodynamic interaction among the microswimmers has been extensively studied both experimentally [19–23] and theoretically [19,24–29]. Some of the former theoretical [21,24,27] and numerical

studies [19,20,22,27] are devoted to the two swimmers' systems. Indeed, all these studies consider pure hydrodynamic interaction among the microswimmers. When the swimmers are far from each other, their interaction can be expressed in terms of a multipole expansion. Conversely, while the swimmers are very close, one needs to use the lubrication theory to calculate their near-field interaction. The former studies revealed that the inclusion of near-field interaction in pair swimming is crucial as it changes the orientation of the swimmers. The theoretical works calculated the near-field interaction using the lubrication theory. On the other hand, the numerical studies used various schemes, namely, Stokesian dynamics [19], boundary element method [22], and lattice Boltzmann simulations [27], to capture the near- and far-field interaction among the swimmers. Several studies on the near- and far-field hydrodynamic interaction between two or more axisymmetric swimmers [19,24] are available where the swimmers change their direction of movement, exhibiting attractive or repulsive behavior depending upon their respective velocity field strengths. The former theoretical works offering accurate calculations of near-field interactions are an essential step toward understanding swimmers' suspension under the nondiluted limit. However, the former studies addressed swimmers with no rotational motion. In contrast, the present study considers the rotational motion of the swimmer as well. The rotational motion causes the nonaxisymmetric part of the flow field in the lubrication region.

In the earlier studies, the popular squirmer model [4,5] has been used to understand the hydrodynamic interactions among swimmers. However, the squirmer model is limited as it can

*Corresponding author: psburada@phy.iitkgp.ac.in

be associated only with the translational motion of the body. Consequently, the body's direction of motion changes either due to the rotational diffusion or the hydrodynamic interaction with another squirmer. In general, many microorganisms can change their direction of movement by rotation of the orientational vector giving rise to helical motion [30]. Notably, the nonaxisymmetric flow feature of a swimmer is common in literature [31–34]. Henceforth, the chiral squirmer model [29,31–36], which is a generalization of the squirmer model, is more applicable for studying the collective behavior of the swimmers. In the latter model, the tangential slip velocity on the surface of a nondeformable spherical body is nonaxisymmetric. As a result, the swimmer can generate chiral flows and helical paths.

Similar to simple squirmers, it has been reported that a pair of chiral squirmers also portray various behaviors, e.g., monotonic divergence, divergence, monotonic convergence, convergence, and even a bounded state [29,37,38] as a result of their mutual hydrodynamic interaction. The helical propulsion of the swimmers leads to this peculiar bounded state, where the swimmers periodically come closer to and distant from each other. It was reported in our earlier work [29]. The later study considered only the far-field hydrodynamic interactions among the squirmers for simplicity, which may not be sufficient to understand the complete interactions among the swimmers. As previously mentioned, the lubrication forces arise when the swimmers are very close to each other, and this influences the collective behavior of the swimmers.

In this article, as an extension of our earlier work [29], we study the combined behavior of two chiral swimmers considering both the near- and the far-field hydrodynamic interactions. We compute the lubrication force between two swimmers when they approach very close to each other. Further, we investigate the complete hydrodynamic behavior of two swimmers. The article is organized as follows. The general chiral squirmer model is briefly discussed in Sec. II. The lubrication force between two swimmers is calculated in Sec. III. The hydrodynamic interaction, both in the near and the far fields, between two swimmers, is discussed in Sec. IV. The influence of the initial conditions of swimmers on their hydrodynamic behavior is explained in Sec. V. The main conclusions are provided in Sec. VI.

II. THE CHIRAL SQUIRMER MODEL

The flow field generated by the low Reynolds number swimmers obeys the Stokes equation [2],

$$\eta \nabla^2 \mathbf{u} = \nabla p, \quad (1)$$

where η is the viscosity, \mathbf{u} is the velocity field, and p is the pressure field which plays the role of a Lagrange multiplier to impose the incompressibility constraint $\nabla \cdot \mathbf{u} = 0$. A chiral squirmer is assumed to be a rigid spherical body of radius a . On its surface, we prescribe a surface slip velocity $\mathbf{S}(\theta, \phi)$ which is tangential to the surface and parametrized by the polar and azimuthal angles θ and ϕ , respectively, in a body-fixed frame defined by three orthogonal unit vectors attached to the sphere center \mathbf{n} , \mathbf{b} , and \mathbf{t} (see Fig. 1). It is convenient to express this surface slip pattern using gradients of spherical harmonics that form a basis for tangential vectors

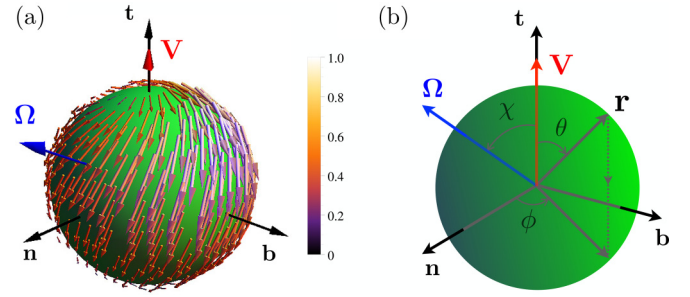


FIG. 1. (a) Example of surface slip velocity patterns of a chiral squirmer in the body-fixed reference frame \mathbf{n} , \mathbf{b} , and \mathbf{t} . Here, we set the velocity and rotation rate of the swimmer as $\mathbf{V} = v(0, 0, 1)$ and $\mathbf{\Omega} = v(1/\sqrt{2}, 0, 1/\sqrt{2})/a$, respectively. The slip coefficients of the second mode are chosen as $\beta_{20}^r = v/3$, $\gamma_{20}^r = v/3$, and the others are zero. (b) Schematic of the body frame of reference (\mathbf{n} , \mathbf{b} , \mathbf{t}) and the corresponding polar and azimuthal angles. The angle between the swimming velocity and the rotation rate is χ .

on the surface [2]. The slip velocity can then be expressed in the form [29,35,36]

$$\mathbf{S}(\theta, \phi) = \sum_{l=1}^{\infty} \sum_{m=-l}^l \left[-\beta_{lm} \nabla_s [P_l^m(\cos \theta) e^{im\phi}] + \gamma_{lm} \hat{\mathbf{r}} \times \nabla_s [P_l^m(\cos \theta) e^{im\phi}] \right], \quad (2)$$

where ∇_s is the gradient operator on the surface of the sphere defined as $\nabla_s = \mathbf{e}_\theta \partial/\partial\theta + (1/\sin\theta)\mathbf{e}_\phi \partial/\partial\phi$, $\hat{\mathbf{r}}$ is the unit vector in radial direction, and $P_l^m(\cos\theta)e^{im\phi}$ are non-normalized spherical harmonics, where $P_l^m(\cos\theta)$ denotes associated Legendre polynomials of order m and degree l . The complex coefficients β_{lm} and γ_{lm} are the mode amplitudes of the prescribed surface slip velocity. We introduce the real and imaginary parts of these amplitudes as $\beta_{lm} = \beta_{lm}^r + im\beta_{lm}^i$ and $\gamma_{lm} = \gamma_{lm}^r + im\gamma_{lm}^i$ with complex conjugates $\beta_{lm}^* = (-1)^m \beta_{l,-m}$ and $\gamma_{lm}^* = (-1)^m \gamma_{l,-m}$, respectively.

The velocity \mathbf{V} and the rotation rate $\mathbf{\Omega}$ of the swimmer can be determined directly using the surface slip velocity, Eq. (2) [39]. They can be expressed in the body-fixed reference frame as $\mathbf{V} = 2(\beta_{11}^r, \beta_{11}^i, \beta_{10}^r)/3$ and $\mathbf{\Omega} = (\gamma_{11}^r, \gamma_{11}^i, \gamma_{10}^r)/a$, respectively. Without loss of generality, the body-fixed reference frame (\mathbf{n} , \mathbf{b} , \mathbf{t}) can be chosen such that \mathbf{t} points in the direction of motion. Accordingly, we have $\beta_{11}^r = \beta_{11}^i = 0$ and we write $\beta_{10}^r = 3v/2$ such that $v = |\mathbf{V}|$ is the speed of the swimmer. Thus, the velocity and rotation rate of the chiral squirmer read [29]

$$\mathbf{V} = vt, \quad (3)$$

$$\mathbf{\Omega} = \frac{\gamma_{11}^r}{a} \mathbf{n} + \frac{\gamma_{11}^i}{a} \mathbf{b} + \frac{\gamma_{10}^r}{a} \mathbf{t}. \quad (4)$$

Also, for simplicity, we choose that the swimmer has rotation rate in the \mathbf{n} - \mathbf{t} plane only. With this choice, we have $\gamma_{11}^i = 0$. In addition, we choose the magnitude of the rotation as $|\mathbf{\Omega}| = v/a$ such that the components of the rotation rate are expressed as $\gamma_{11}^r/a = (v/a) \sin \chi$, $\gamma_{11}^i/a = 0$, and $\gamma_{10}^r/a = (v/a) \cos \chi$, where χ is the angle between \mathbf{V} and $\mathbf{\Omega}$. The corresponding flow field and the pressure field of the swimmer can be obtained by solving Eq. (1) with the surface

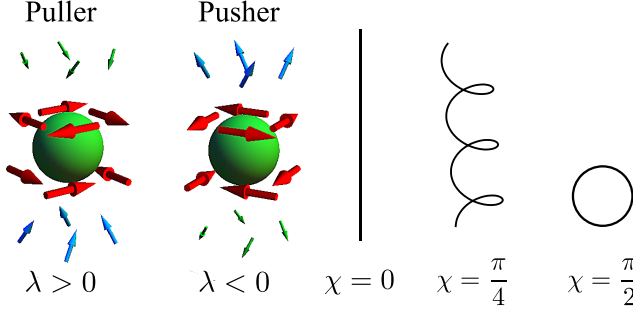


FIG. 2. Chiral flow pattern exhibited by a puller and a pusher type chiral squirmer in three dimensions, for $\lambda = 3\beta_{20}^r = 3\gamma_{20}^r$ in Eq. (5), and the chiral squirmer's path for different angles χ between the velocity \mathbf{V} and the rotation rate $\mathbf{\Omega}$. The initial velocities and rotation rates of both the swimmers are set to $v(0, 0, 1)$ and $v(\sin \chi, 0, \cos \chi)/a$, respectively. For the flow patterns we set $\chi = \pi/4$ and $\lambda = v$ for puller, and $\chi = \pi/4$ and $\lambda = -v$ for pusher.

slip [Eq. (2)] in the laboratory frame of reference (**lf**). They read [29]

$$\begin{aligned} \mathbf{u}_{\text{lf}}(\mathbf{r}) = & \frac{3v}{2} \frac{a^3}{r^3} \left[P_1(\mathbf{t} \cdot \hat{\mathbf{r}}) \hat{\mathbf{r}} - \frac{\mathbf{t}}{3} \right] + 3\beta_{20}^r \left(\frac{a^4}{r^4} - \frac{a^2}{r^2} \right) P_2(\mathbf{t} \cdot \hat{\mathbf{r}}) \hat{\mathbf{r}} \\ & + \beta_{20}^r \frac{a^4}{r^4} P_2'(\mathbf{t} \cdot \hat{\mathbf{r}}) [(\mathbf{t} \cdot \hat{\mathbf{r}}) \hat{\mathbf{r}} - \mathbf{t}] \\ & - \gamma_{20}^r \frac{a^3}{r^3} P_2'(\mathbf{t} \cdot \hat{\mathbf{r}}) \mathbf{t} \times \hat{\mathbf{r}}, \end{aligned} \quad (5)$$

$$p_{\text{lf}}(\mathbf{r}) = -2\eta\beta_{20}^r \frac{a^2}{r^3} P_2(\mathbf{t} \cdot \hat{\mathbf{r}}), \quad (6)$$

where \mathbf{t} is the swimming direction, r is the distance from the center of the swimmer where the flow field is determined, $\hat{\mathbf{r}} = \mathbf{r}/r$ is the radial vector, $P_2(x)$ denotes a second-order Legendre polynomial, and $P_2' = dP_2/dx$ with $x = \mathbf{t} \cdot \hat{\mathbf{r}} = \cos \theta$. Note that in Eq. (5) the higher order terms $l > 2$ are being ignored as their contribution is negligible in the current study. To have a minimal model, in Eq. (5) we have ignored $l = 2$ modes with $m \neq 0$. However, it is straightforward to include the additional terms in the analysis. Depending on the sign of the ratio $\beta = \beta_{20}^r/\beta_{10}^r$, the swimmer can be classified as a puller (for $\beta > 0$) or pusher (for $\beta < 0$) type (see Fig. 2). While pullers have an extensile force dipole, resulting, e.g., from the front part of the body, pushers have a contractile force dipole arising, e.g., from the rear part of the body [9] (see Fig. 2). Note that the flow field in the body frame (**bf**) can be obtained from that in the laboratory frame (**lf**) as $\mathbf{u}_{\text{bf}}(\mathbf{r}) = \mathbf{u}_{\text{lf}}(\mathbf{r}) - \mathbf{V} - \mathbf{\Omega} \times \mathbf{r}$.

The equations of motion of the swimmer can be obtained using the force and torque balance conditions [40]. They read

$$\dot{\mathbf{q}} = \mathbf{V}, \quad \dot{\mathbf{n}} = \mathbf{\Omega} \times \mathbf{n}, \quad \dot{\mathbf{b}} = \mathbf{\Omega} \times \mathbf{b}, \quad \dot{\mathbf{t}} = \mathbf{\Omega} \times \mathbf{t}, \quad (7)$$

where \mathbf{q} is the position of the swimmer in the laboratory frame of reference and the dot represents the derivative with respect to time. For $\mathbf{V} \parallel \mathbf{\Omega}$, we get $\chi = 0$, and the resulting swimming path of the swimmer is a straight line. In this case, the swimmer rotates around the axis of motion. For $\chi = \pi/2$, the swimmer moves in a circular path in a plane. For other values of χ , the path is a helix (see Fig. 2) [29]. Note that

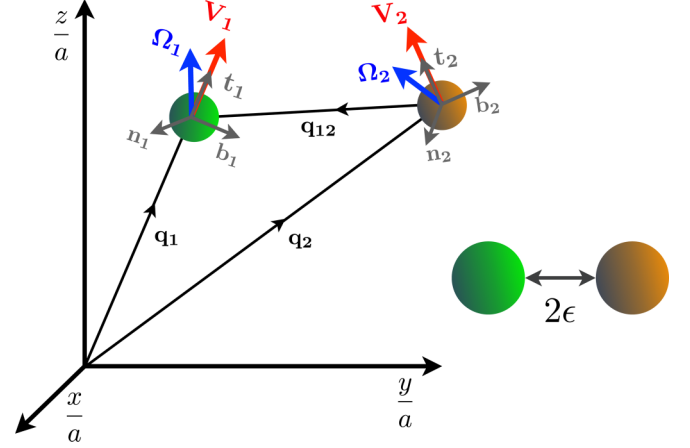


FIG. 3. Schematic representation of two chiral swimmers in the laboratory frame of reference. When swimmers are close to each other, i.e., the distance between them $R = |\mathbf{q}_{ij}| = r \leq 2(a + \epsilon)$, where a is the radius of the swimmer, then the lubrication forces control the hydrodynamic behavior of the swimmers. Otherwise, the far-field hydrodynamic interactions dominate.

Eq. (7) determines the motion of a single isolated squirmer, whereas for a pair of swimmers we need to take into account the hydrodynamic interaction between them which we study in the following.

III. LUBRICATION FORCE BETWEEN TWO CHIRAL SWIMMERS

Substantial work has been done in low Reynolds number swimming near an air-liquid interface [41–44]. To find the force on the body near the air-liquid interface, considering perfect slip, a mirror image technique has been used [43,44]. To calculate the lubrication force between two swimmers, a similar approach can be adapted. Here, in place of an image, both the swimmers are real, and their dynamics is controlled by the Stokes equation (see Fig. 3). However, in the lubrication region, the Stokes equation is modified (see Appendix A). Taking into account the active surface velocity of both the swimmers as boundary conditions, we can find the lubrication flows around the swimmers from the solution of the modified Stokes equation. The lubrication force acting on a swimmer can be calculated by knowing the velocity field of the nearby swimmer (for details, see Appendix A). The component of the lubrication force acting on a swimmer along its swimming direction reads

$$F_z \approx \frac{3\pi B a^2}{2} \ln \epsilon, \quad (8)$$

where $B = \beta_{10}^r t_{13} - \beta_{10}^r t_{23}$, ϵ is half the distance between the swimmers, $t_{13} = \mathbf{t}_1 \cdot \mathbf{e}_z$, $t_{23} = \mathbf{t}_2 \cdot \mathbf{e}_z$, \mathbf{e}_z is the unit vector along the Z direction, and \mathbf{t}_1 and \mathbf{t}_2 are the orientation vectors of swimmers one and two, respectively (for details, see Appendix A). Taking into account the solution for squeezing motion of two rigid spheres, we can find the velocity of the axisymmetric squirmer in the lubrication region as $U \sim \epsilon \ln \epsilon$ [43,45]. Similarly, the velocity of the chiral squirmer can be

obtained as

$$U = -2a^2 B \epsilon \ln \epsilon. \quad (9)$$

Also, note that the lubrication torques are of the order $O(\epsilon^{1/2})$, and can be neglected in the limit $\epsilon \rightarrow 0$.

Notably, the results obtained here agree with those by Wang and Ardekani [43]. However, the latter is the case of axisymmetric squirmers, whereas the present study deals with chiral squirmers. The flow field in the narrow gap between the axisymmetric squirmers contains only radial and polar components. However, for the chiral squirmers, the flow field in the lubrication region contains an azimuthal component in addition to the radial and polar components. Note that the lubrication force acting on the case of axisymmetric squirmers contains the polar slip coefficients only. On the other hand, the lubrication torque contains the azimuthal slip coefficients for a chiral squirmer. However, the contribution from the lubrication torque is insignificant in the hydrodynamic interaction of chiral squirmers. Consequently, the calculated lubrication forces are the same for both axisymmetric and chiral squirmers despite having different flow fields.

In the presence of the lubrication force, the corresponding equations of motion of the swimmers are given by

$$\dot{\mathbf{q}}_i = \mathbf{V}_i + \mathbf{U}_i^{\text{lub}} + \sum_{j=1; i \neq j}^2 \mathbf{u}_j(\mathbf{q}_{ij}, \mathbf{n}_j, \mathbf{b}_j, \mathbf{t}_j),$$

$$\begin{bmatrix} \dot{\mathbf{n}}_i \\ \dot{\mathbf{b}}_i \\ \dot{\mathbf{t}}_i \end{bmatrix} = \begin{bmatrix} \boldsymbol{\Omega}_i + \sum_{j=1; i \neq j}^2 \boldsymbol{\omega}_j(\mathbf{q}_{ij}, \mathbf{n}_j, \mathbf{b}_j, \mathbf{t}_j) \\ \mathbf{n}_i \\ \mathbf{b}_i \\ \mathbf{t}_i \end{bmatrix}, \quad (10)$$

where $\mathbf{U}_i^{\text{lub}} = U_z(\cos \theta' \mathbf{t}_i - \sin \theta' \mathbf{n}_i)$ is the additional velocity contribution arising due to the other swimmer in the lubrication region, $\theta' = \cos^{-1}(\mathbf{t}_i \cdot \mathbf{e}_z)$, and the vorticity field $\boldsymbol{\omega} = (\nabla \times \mathbf{u})/2$. Note that $\mathbf{U}_i^{\text{lub}} = 0$ for $R > 2(a + \epsilon)$, and $\mathbf{V}_i + \sum_{j=1; i \neq j}^2 \mathbf{u}_j = \sum_{j=1; i \neq j}^2 \boldsymbol{\omega}_j = 0$ for $R \leq 2(a + \epsilon)$, where $\epsilon \ll a$ and $R = |\mathbf{q}_{ij}|$ is the radial distance between the squirmers.

IV. HYDRODYNAMIC BEHAVIOR OF TWO CHIRAL SWIMMERS

To study the hydrodynamic interaction between two swimmers we numerically solve Eq. (10), using ode15s in MATLAB software, to calculate the trajectories of two chiral swimmers and investigate their combined behavior. For simplicity, we consider chiral swimmers having translational velocities of equal magnitudes, i.e., $|\mathbf{V}_1| = |\mathbf{V}_2| = v$. The rotation rates of the swimmers are, in general, different and read $\boldsymbol{\Omega}_1 = v(\sin \chi_1, 0, \cos \chi_1)/a$ for swimmer one and $\boldsymbol{\Omega}_2 = v(\sin \chi_2, 0, \cos \chi_2)/a$ for swimmer two. Note that changes in χ_1 and χ_2 modify the corresponding torsion and curvature of the swimmers' helical trajectories. Also, $l > 1$ modes in the velocity field Eq. (5) play a crucial role in the hydrodynamic interaction between the swimmers. As mentioned earlier, we consider up to $l = 2$ modes in the flow field. We choose $l = 2$ modes corresponding to swimmer one as $3\beta_{20}^r = 3\gamma_{20}^r = \lambda_1$ and similarly for swimmer two as $3\beta_{20}^r = 3\gamma_{20}^r = \lambda_2$. Note that for $\lambda_1 \neq \lambda_2$, the swimmers differ in their chiral flows that

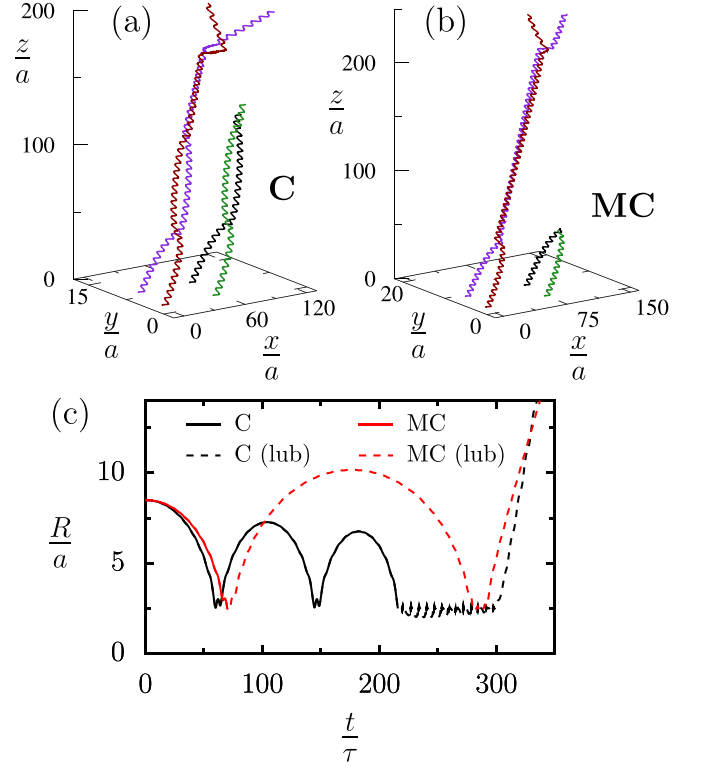


FIG. 4. Panel (a) shows the trajectories of two converging (C) swimmers in the absence of near-field interaction (green and black helices shifted by 70 units along the x direction) and in the presence of it (purple and red). Similarly, panel (b) shows the trajectories of two monotonically converging (MC) swimmers in the absence and in the presence of near-field interactions. Panel (c) shows the corresponding distance R between two hydrodynamically interacting swimmers as a function of time both in the absence and in the presence of the lubrication force. Here, lengths are scaled by the radius of the swimmer a and time scaled by $\tau = v/a$. Note that lubrication forces convert the monotonic convergence (MC) and convergence states (C) into divergence state (D). Here, for the state C, we choose $\chi_1 = \chi_2 = \pi/6$, $\lambda_1 = -2.5$, and $\lambda_2 = 2.5$. For MC, we choose $\chi = \pi/6$, $\lambda_1 = -2$, and $\lambda_2 = 2$

they generate. Thus, variation in χ_i and $\pm\lambda_i$ ($i = 1, 2$) determines the nature of the interaction between the swimmers and gives rise to several interesting swimming characteristics. As mentioned earlier, the sign of λ_i [see Eq. (5)] decides the nature of the swimmer, i.e., pusher or puller type. Accordingly, we consider the subcases, i.e., pusher-pusher: $(-\lambda_1, -\lambda_2)$; puller-puller: (λ_1, λ_2) ; pusher-puller: $(-\lambda_1, \lambda_2)$; and puller-pusher: $(\lambda_1, -\lambda_2)$. We have considered various possible initial configurations for the swimmers. Out of all, in this article, we present only the planar configuration, where both the swimmers start initially on the xy plane, by a distance R_0 , moving in the positive z direction. In the planar configuration, swimmers get enough time to interact with each other, whereas it may not be the case in other configurations. This particular choice of the configuration recovers the known behaviors exhibited by two simple squirmers (without chirality) and some additional exciting behaviors discussed below.

Note that the hydrodynamic interaction between two chiral swimmers in the far-field limit has been explored in the

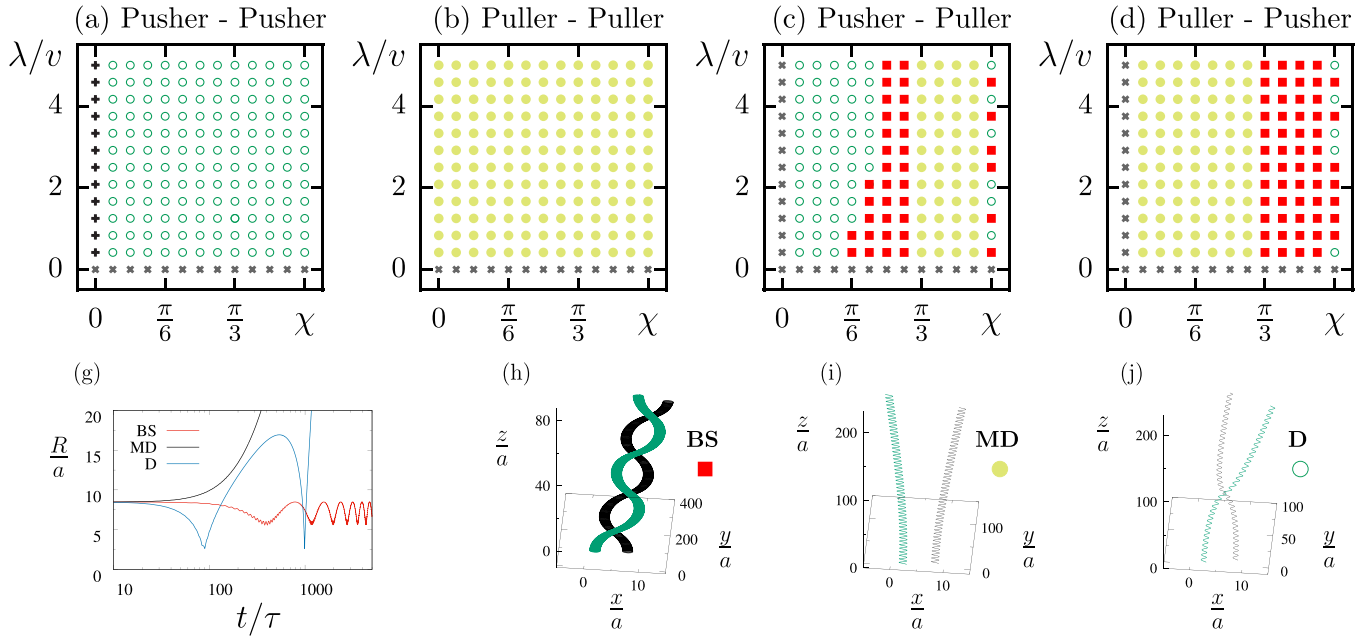


FIG. 5. (a)–(d) Swimming states of two hydrodynamically interacting chiral swimmers of various combinations, i.e., pusher or puller. Hollow circles: Divergence (D); solid circles: Monotonic divergence (MD); squares: Bounded (BS), cross: Parallel swimming; and plus: Forbidden states. (e) The corresponding distance R between the swimmers is plotted as a function of time t . (f)–(h) Swimming trajectories corresponding to different states, for the values $\chi = \pi/3$ and $(\lambda_1, \lambda_2) = v(1, -1)$ for BS, $\chi = \pi/3$ and $(\lambda_1, \lambda_2) = v(-1, 1)$ for MD, and $\chi = 5\pi/12$ and $(\lambda_1, \lambda_2) = v(-1, -1)$ for D. Here, lengths are scaled by radius of the swimmer a , time scaled by $\tau = v/a$, and velocity with v . The initial position of swimmer one is $(9, 9, 0)a$ and for swimmer two is $(3, 3, 0)a$. The initial velocities and rotation rates of both the swimmers are set to $v(0, 0, 1)$ and $(v/a)(\sin \chi, 0, \cos \chi)$, respectively.

previous work [29]. Five different swimming states were observed: (i) bounded (BS) [see Fig. 5(h)], in which the swimmers oscillate around an average trajectory, (ii) monotonic divergence (MD) [see Fig. 5(i)], in which the swimmers drift away from each other from the beginning, (iii) divergence (D) [see Fig. 5(j)], in which initially the swimmers are attracted to each other, but in the long-time limit, they move away from each other due to the growing repulsion between them, (iv) monotonic convergence (MC) [Fig. 4(b)], in which the swimmers due to strong attraction monotonically approach each other at a distance where near-field interaction is more crucial than the far-field interaction, and (v) convergence (C) [Fig. 4(a)], in which the swimmers initially oscillate about an average trajectory and then converge towards each other due to the hydrodynamic attraction between them. However, if the near-field interactions are dominant, as in the case of a dense suspension, then the fate of the last two states, say, MC and C, were unknown. In this work, as mentioned earlier, we consider both the near- and the far-field interactions to get the complete hydrodynamic behavior of two chiral swimmers. Figure 4 depicts the behavior of two chiral swimmers, which exhibit attractive behavior in the absence and in the presence of the lubrication forces. Due to the lubrication force, the C [Fig. 4(a)] and MC [Fig. 4(b)] states are converted into the D state (see Fig. 4). Note that the lubrication force is repulsive in nature. As a result, as the swimmers approach each other, i.e., as $R \leq 2(a + \epsilon)$ [see Eq. (10)], they start to repel each other and diverge.

Figure 5 shows the hydrodynamic behavior of two identical chiral swimmers. Here, we set $\chi_1 = \chi_2 = \chi$ and $|\lambda_1| =$

$|\lambda_2| = \lambda$, i.e., the relative orientations of the swimmers with respect to their motion and the strength of the hydrodynamic flow fields of both swimmers are identical. As mentioned earlier, due to the lubrication force, which is repulsive in nature, MC and C states do not survive, leaving mainly D, MD, and BS states in the state diagrams. Note that for the pusher-puller combination, for $\chi = 0$, we obtain forbidden states (black plus). Two pushers swimming in parallel lines attract each other and may converge to a locked state, considered as a numerical artifact. However, for $\chi \neq 0$, the pushers move in a helical path, and the locked state does not appear.

Note that in the case of axisymmetric swimmers (simple squirmers), the combination of pusher-puller and puller-puller-type swimmers would exhibit similar hydrodynamic behavior. However, in the case of nonaxisymmetric swimmers (chiral squirmers), the same combination would not exhibit a similar hydrodynamic behavior [29]. It is because the flow pattern of a puller-type chiral swimmer is different from a pusher-type chiral swimmer, which makes the squirmers' bounded motion depend on the pusher's relative position and puller. The parameters λ_1 , λ_2 , χ_1 , and χ_2 can be varied to study the hydrodynamic behavior of two chiral swimmers (see Fig. 9 in Appendix B for more details).

For the choice $\chi_1 = \chi_2 = \pi/2$, swimmers move in a plane. In this case, an isolated swimmer moves in a closed circular path with no net displacement [see Fig. 6(a)]. However, the presence of a second swimmer in its proximity changes its movements dramatically. The hydrodynamic forces from the second swimmer convert the two-dimensional circular swimming into three-dimensional helical swimming [see Figs. 6(b)

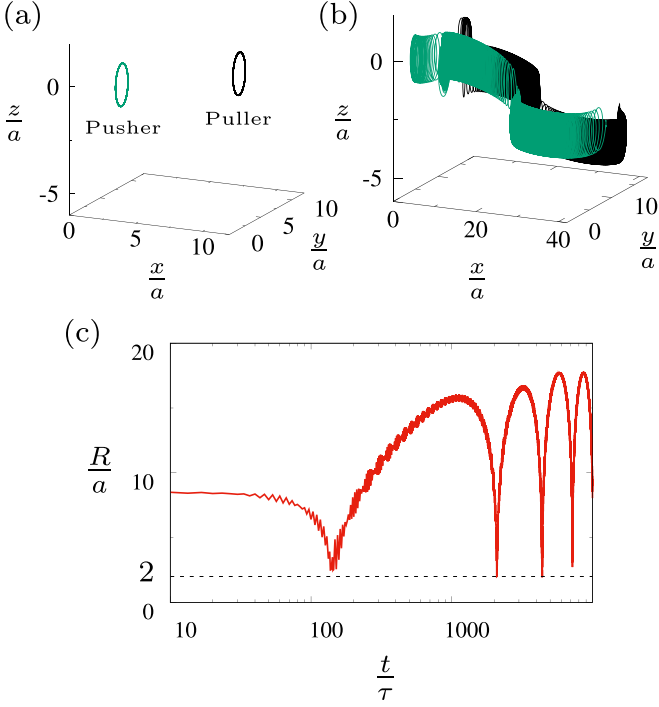


FIG. 6. (a) Circular motion of two swimmers in the absence of the lubrication force. (b) Bounded motion of two swimmers in the presence of the lubrication force. The corresponding distance between the swimmers as a function of time is shown in (c). The dashed line in (c) indicates the minimum distance that the swimmers can approach. Here, we set $\lambda = 55/12$ and $\chi = \pi/2$ and the initial positions of the swimmers as $(3,3,0)$ (puller) and $(9,9,0)$ (pusher). Here, lengths are scaled by radius of the swimmer a and time scaled by $\tau = v/a$.

and 6(c)]. Though in some situations, the pair of swimmers perform a bounded motion; however, in other situations, they drift away from each other in the long-time limit (see Fig. 5). These behaviors are therefore sensitive to the strength of the flow fields (λ) and the associated lubrication force. Note that the origin of the bounded motion, in this situation, is the lubrication force acting between the swimmers. However, the bounded motion is less stable here, and in some cases, the swimmers diverge from each other in drifting circular paths. Note that, for other values of χ , the bounded motion occurs due to the helical propulsion of the swimmers, and χ plays a more crucial role than λ there. Consequently, the former bounded motion is more stable compared to the ones observed due to the lubrication forces.

Notably, a bound state was observed experimentally for a pair of spinning bottom-heavy *Volvox* due to the combined interface effect, gravity, and lubrication forces [20–22]. Here, the bound state is observed for three-dimensional chiral swimmers due to far-field hydrodynamic interaction among them. Note that the bounded motion is restricted to parallel swimming with equal strength of flow field of chiral swimmers, i.e., swimmers with identical χ and λ (see Figs. 5 and 9). However, for certain situations, say, $\chi_1 = \chi_2 = \pi/2$, we encounter bound states originating from the combined effect of lubrication force and hydrodynamic attraction.

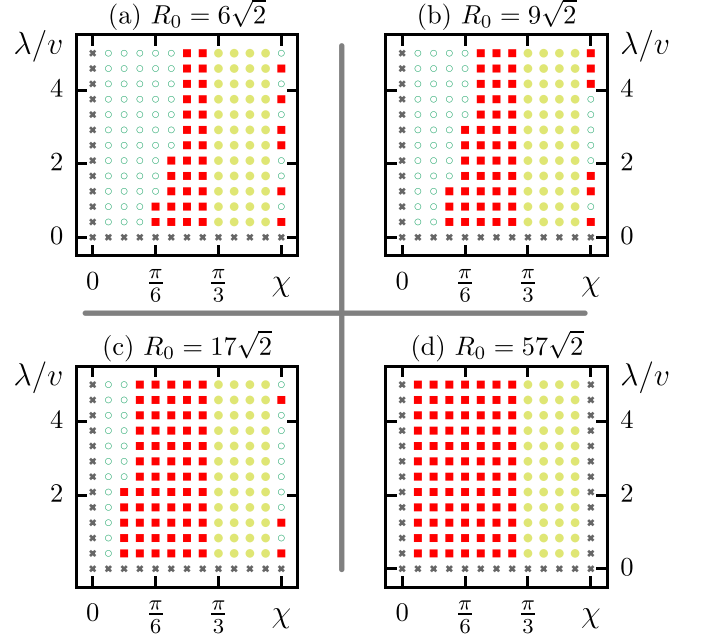


FIG. 7. Numerically obtained swimming behaviors of pusher-puller-type chiral swimmers with different initial positions. The corresponding initial distance is R_0 . (a) For $\mathbf{q}_1 = (9, 9, 0)a$ and $\mathbf{q}_2 = (3, 3, 0)a$ [as in Fig. 5(c)], (b) for $\mathbf{q}_1 = (12, 12, 0)a$ and $\mathbf{q}_2 = (3, 3, 0)a$, (c) for $\mathbf{q}_1 = (20, 20, 0)a$ and $\mathbf{q}_2 = (3, 3, 0)a$, and (d) for $\mathbf{q}_1 = (60, 60, 0)a$ and $\mathbf{q}_2 = (3, 3, 0)a$. Swimmers have the same initial velocity $\mathbf{V}_1 = \mathbf{V}_2 = v(0, 0, 1)$ and rotation rate $\mathbf{\Omega}_1 = \mathbf{\Omega}_2 = v(\cos \chi, 0, \sin \chi)/a$, which depends on the angle χ . Symbols are the same as in Fig. 5.

V. INFLUENCE OF THE INITIAL CONFIGURATION OF THE SWIMMERS

In this section, we study the impact of the initial distance R_0 between the swimmers on their hydrodynamic behavior. As a test case, we consider the pusher-puller combination (see Fig. 7). The nature of hydrodynamic interaction between the swimmers changes with varying R_0 . As R_0 increases, swimmers exhibit mainly BS, D, and MD states. Due to the lubrication forces, the states C or MC do not appear in the state diagrams. As R_0 increases, swimmers tend to exhibit BS states more than MD. The general tendency of the swimmers is to be repulsive or attractive. For purely repulsive situations, swimmers exhibit an MD state. If swimmers tend to exhibit attractive behavior, then based on their near-field interactions, the swimming behavior can be classified as D or BS. With increasing R_0 , the flow field of the swimmers prohibits them from approaching close to each other. Thus, swimmers exhibit bounded states only. Note that the lubrication forces become redundant for higher R_0 values. For $\chi = \pi/2$, swimmers exhibit bounded states between the MD states, depending on the strength of λ , at lower R_0 values. However, as R_0 increases, these D states are converted into BS states. In the other combination of swimmers, e.g., pusher-pusher or puller-puller, MD states do not alter with respect to R_0 . However, for smaller R_0 , swimmers mostly remain in the D state. With increasing R_0 (intermediate region), the probability that the swimmers will be bounded to each other increases (see Fig. 7). If R_0

is very high ($\sim 10^3$), the swimmers never approach each other very close, so they cannot interact effectively. Also, swimmers moving in straight lines or having no stresslet do not interact with each other (gray cross symbols in the state diagrams). Note that for $R_0 \sim 10^3$, the hydrodynamic interaction becomes ineffective.

Note that, as reported in our earlier work [29], the bound state is stable even with a small perturbation to their initial orientation, say, $(-0.006\pi/24) \leq \psi_1 \leq (0.007\pi/24)$, $(-0.007\pi/24) \leq \psi_2 \leq (0.007\pi/24)$, and $(-1.4\pi/24) \leq \psi_3 \leq (\pi/24)$. Beyond this range, the BS states are converted into divergence states. Here, ψ_1 , ψ_2 , and ψ_3 are initial rotations about \mathbf{t}_2 , \mathbf{b}_2 , and \mathbf{n}_2 axes, respectively. Notably, $(\mathbf{n}_1, \mathbf{b}_1, \mathbf{t}_1)$ and $(\mathbf{n}_2, \mathbf{b}_2, \mathbf{t}_2)$ are material frames of reference of the first and second swimmers. While the first swimmer is initially aligned along the z axis, the initial orientation of the second swimmer is perturbed by (ψ_1, ψ_2, ψ_3) . Note that D and MD states are not influenced by the initial perturbation in the orientation of the swimmers.

VI. CONCLUSIONS

In this article, we have determined the near-field interaction between the two chiral swimmers using the lubrication theory. The hydrodynamic force and the torque on a swimmer due to the presence of another swimmer have been determined analytically in the lubrication region. The hydrodynamic behavior of a pair of swimmers has been analyzed by solving their respective equations of motion numerically using the ode15s in MATLAB. When the swimmers approach very close, the lubrication force drives the swimmers away from each other within the long-time limit. Consequently, due to near- and far-field hydrodynamic interactions, two chiral swimmers exhibit only monotonic divergence, divergence, and bounded states. We find that the coupling of near- and far-field hydrodynamic interactions converts the planar circular movement of a swimmer, observed for $\chi = \pi/2$, into three-dimensional helical swimming. It leads to an unstable bounded motion of a pair of swimmers. However, the stable bounded motion of the swimmers, observed for $\chi < \pi/2$, is solely due to the far-field hydrodynamic interaction between the swimmers. This study helps to understand the collective behavior of ciliated microorganisms and artificial swimmers [46–50].

ACKNOWLEDGMENT

This work was supported by the Indian Institute of Technology Kharagpur, India.

APPENDIX A: LUBRICATION FORCE

We briefly explain here the lubrication calculations [43]. When the spherical swimmers approach each other, i.e., $R < 2(a + \epsilon)$, the narrow gap between them forms a cylindrical region (see Fig. 8). Here, R is the distance between the swimmer, a is the radius of the swimmer, and ϵ is half of the distance between the swimmers. Note that we assume the thin interaction layer near the surface, over which the slip boundary condition is assumed, is thin compared to the gap size [24]. Both the squirmers are situated on two opposite sides

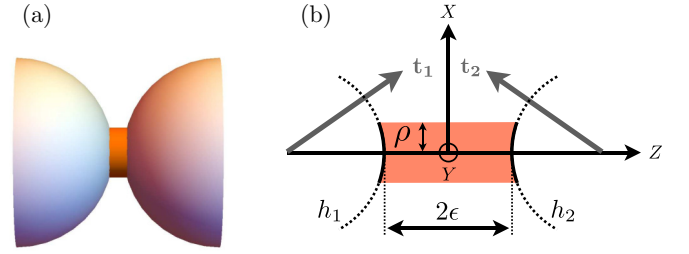


FIG. 8. (a) Schematic diagram of the lubrication region. (b) Schematic of the cylindrical region of length 2ϵ between the spherical swimmers. Here, ρ is the radius of the cylinder; X , Y , and Z form the Cartesian frame whose origin is at the middle of the parabolic surfaces h_1 and h_2 ($h_2 = -h_1$) of swimmers one and two, respectively. The corresponding radial vector is defined as $\boldsymbol{\rho} = X\mathbf{e}_X + Y\mathbf{e}_Y = \rho\mathbf{e}_\rho$, where \mathbf{e}_ρ is the unit radial vector, and \mathbf{e}_ϕ is the unit vector along the azimuthal direction (on the XY plane) in the cylindrical region. \mathbf{t}_1 and \mathbf{t}_2 are the orientations of the swimmers.

of an imaginary plane and generate surface motion relative to that plane. We consider the coordinate system lying on this plane. The flow fields generated by the swimmers obey the Stokes equation, Eq. (1), in this region. The surfaces of the two spherical swimmers in the narrow gap region can be considered as parabolic surfaces having the form

$$h_1 = \epsilon + \frac{\rho'^2}{2} + \dots, \quad (\text{A1})$$

$$h_2 = -h_1, \quad (\text{A2})$$

where ρ' is the dimensionless radius in cylindrical coordinates. We set the origin at the midpoint between two spherical squirmers. The stretched coordinates (X, Y, Z) [43] used here are defined as [see Fig. 8(b)],

$$\begin{aligned} \sqrt{\epsilon}X &= x, & \sqrt{\epsilon}Y &= y, & \epsilon Z &= z, \\ \rho' &= \sqrt{x^2 + y^2}, & \sqrt{\epsilon}\rho &= \rho'. \end{aligned} \quad (\text{A3})$$

Accordingly, the scaled surfaces are defined as $H_1 = h_1/\epsilon$ and $H_2 = h_2/\epsilon = -H_1$. The radial vector in the stretched coordinates is defined as $\boldsymbol{\rho} = X\mathbf{e}_X + Y\mathbf{e}_Y = \rho\mathbf{e}_\rho$, where \mathbf{e}_ρ is the unit radial vector. The Stokes equation, Eq. (1), in the stretched coordinates can be expressed in dimensionless form as

$$\left[\epsilon \left(\frac{\partial^2}{\partial X^2} + \frac{\partial^2}{\partial Y^2} \right) + \frac{\partial^2}{\partial Z^2} \right] \mathbf{u} = \epsilon \left(\epsilon^{1/2} \frac{\partial p}{\partial X}, \epsilon^{1/2} \frac{\partial p}{\partial Y}, \frac{\partial p}{\partial Z} \right), \quad (\text{A4})$$

$$\epsilon^{1/2} \left(\frac{\partial u}{\partial X} + \frac{\partial v}{\partial Y} \right) + \frac{\partial w}{\partial Z} = 0, \quad (\text{A5})$$

where u , v , and w are the components of the velocity field, and p is the pressure field.

The surface slip [Eq. (2)] of swimmer one, for the $l = 1$ mode, is given by

$$\mathbf{u}^{\text{sl}} = -\beta_{10}^r [(\mathbf{t}_1 \cdot \mathbf{e}_r)\mathbf{e}_r - \mathbf{t}_1] - (\mathbf{t}_1 \times \mathbf{e}_r)\gamma_{10}^r, \quad (\text{A6})$$

where \mathbf{t}_1 is the swimming direction and \mathbf{e}_r is the unit radial vector measured from the center of swimmer one. Similarly,

for swimmer two,

$$\mathbf{u}^{\text{s}2} = -\beta_{10}^{r2}[(\mathbf{t}_2 \cdot \mathbf{e}'_r)\mathbf{e}'_r - \mathbf{t}_2] - (\mathbf{t}_2 \times \mathbf{e}'_r)\gamma_{10}^{r2}, \quad (\text{A7})$$

where \mathbf{t}_2 is the swimming direction and \mathbf{e}'_r is the unit radial vector measured from the center of swimmer two. Following the procedure given by Ishikawa *et al.* [24], we expand the velocity and pressure fields on the surface of the swimmer in terms of $\epsilon^{1/2}$ as

$$\mathbf{u}^{\text{s}} = \mathbf{u}_0^{\text{s}} + \epsilon^{1/2}\mathbf{u}_1^{\text{s}} + \dots, \quad (\text{A8})$$

$$p = p_\infty + \epsilon^{-3/2}(p_0 + \epsilon^{1/2}p_1 + \dots). \quad (\text{A9})$$

Similarly, the surface slip of swimmers one and two can be expanded in terms of $\epsilon^{1/2}$ as $\mathbf{u}^{\text{s}1} = \mathbf{u}_0^{\text{s}1} + \epsilon^{1/2}\mathbf{u}_1^{\text{s}1} + \dots$ and $\mathbf{u}^{\text{s}2} = \mathbf{u}_0^{\text{s}2} + \epsilon^{1/2}\mathbf{u}_1^{\text{s}2} + \dots$, respectively, where

$$\mathbf{u}_0^{\text{s}1} = \beta_{10}^{r1}[(\mathbf{t}_1 \cdot \mathbf{e}_z)\mathbf{e}_z - \mathbf{t}_1] + (\mathbf{t}_1 \times \mathbf{e}_z)\gamma_{10}^{r1}, \quad (\text{A10})$$

$$\mathbf{u}_1^{\text{s}1} = \beta_{10}^{r1}[(\mathbf{t}_1 \cdot \boldsymbol{\rho})\mathbf{e}_z + (\mathbf{t}_1 \cdot \mathbf{e}_z)\boldsymbol{\rho}] - (\mathbf{t}_1 \times \boldsymbol{\rho})\gamma_{10}^{r1}, \quad (\text{A11})$$

$$\mathbf{u}_0^{\text{s}2} = -\beta_{10}^{r2}[(\mathbf{t}_2 \cdot \mathbf{e}_z)\mathbf{e}_z - \mathbf{t}_2] - (\mathbf{t}_2 \times \mathbf{e}_z)\gamma_{10}^{r2}, \quad (\text{A12})$$

$$\mathbf{u}_1^{\text{s}2} = \beta_{10}^{r2}[(\mathbf{t}_2 \cdot \boldsymbol{\rho})\mathbf{e}_z + (\mathbf{t}_2 \cdot \mathbf{e}_z)\boldsymbol{\rho}] - (\mathbf{t}_2 \times \boldsymbol{\rho})\gamma_{10}^{r2}. \quad (\text{A13})$$

Here, $\mathbf{t}_1 = t_{11}\mathbf{e}_X + t_{12}\mathbf{e}_Y + t_{13}\mathbf{e}_Z$ and $\mathbf{t}_2 = t_{21}\mathbf{e}_X + t_{22}\mathbf{e}_Y + t_{23}\mathbf{e}_Z$. Note that \mathbf{e}_X , \mathbf{e}_Y , and \mathbf{e}_Z are the unit vectors along the stretched coordinates X , Y , and Z , respectively.

Following the procedure by Wang and Ardekani [43], we get the solutions for the velocity and pressure fields in the lubrication region. We found that, in the lubrication region, only the first-order term survives in the solution of the pressure field, and the contribution from the other terms is negligible in the limit $\epsilon \rightarrow 0$. To the first order, the lubrication equations for the given system are

$$\frac{\partial p_1}{\partial X} = \frac{\partial^2 u_1}{\partial Z^2}, \quad (\text{A14a})$$

$$\frac{\partial p_1}{\partial Y} = \frac{\partial^2 v_1}{\partial Z^2}, \quad (\text{A14b})$$

$$\frac{\partial p_1}{\partial Z} = 0, \quad (\text{A14c})$$

where u_1 , v_1 , and p_1 are the components of the velocity and pressure fields, respectively, corresponding to the first terms [see Eqs. (A8) and (A9)].

As the velocity field is equal to the active slip at the surface of the swimmer, the corresponding components (first order) of the surface slip of swimmer one read

$$u_{11} = \mathbf{u}_1^{\text{s}1} \cdot \mathbf{e}_X = \beta_{10}^{r1}t_{13}X + \gamma_{10}^{r1}t_{13}Y, \quad (\text{A15a})$$

$$v_{11} = \mathbf{u}_1^{\text{s}1} \cdot \mathbf{e}_Y = \beta_{10}^{r1}t_{13}Y - \gamma_{10}^{r1}t_{13}X, \quad (\text{A15b})$$

$$w_{11} = \mathbf{u}_1^{\text{s}1} \cdot \mathbf{e}_Z = \beta_{10}^{r1}(\mathbf{t}_1 \cdot \mathbf{e}_\rho)\rho + \gamma_{10}^{r1}\rho(\mathbf{t}_1 \cdot \mathbf{e}_\phi), \quad (\text{A15c})$$

where \mathbf{e}_ϕ is the unit vector along the azimuthal direction (on the XY plane) in the cylindrical region. Similarly, the components of the surface slip of swimmer two read

$$u_{21} = \mathbf{u}_1^{\text{s}2} \cdot \mathbf{e}_X = -\beta_{10}^{r2}t_{23}X + \gamma_{10}^{r2}t_{23}Y, \quad (\text{A16a})$$

$$v_{21} = \mathbf{u}_1^{\text{s}2} \cdot \mathbf{e}_Y = -\beta_{10}^{r2}t_{23}Y - \gamma_{10}^{r2}t_{23}X, \quad (\text{A16b})$$

$$w_{21} = \mathbf{u}_1^{\text{s}2} \cdot \mathbf{e}_Z = -\beta_{10}^{r2}(\mathbf{t}_2 \cdot \mathbf{e}_\rho)\rho + \gamma_{10}^{r2}\rho(\mathbf{t}_2 \cdot \mathbf{e}_\phi). \quad (\text{A16c})$$

Note that, in a laboratory frame of reference, the velocity field is zero, i.e., $\mathbf{u} = 0$, far away from the swimmers. Integrating Eq. (A14) twice, we get

$$u_1 = \frac{Z^2 - H_1^2}{2} \frac{\partial p_1}{\partial X} + \frac{Z}{2H_1}(u_{11} - u_{21}) + \frac{1}{2}(u_{11} + u_{21}), \quad (\text{A17a})$$

$$v_1 = \frac{Z^2 - H_1^2}{2} \frac{\partial p_1}{\partial Y} + \frac{Z}{2H_1}(v_{11} - v_{21}) + \frac{1}{2}(v_{11} + v_{21}). \quad (\text{A17b})$$

Now, differentiating Eq. (A17a) with respect to X and Eq. (A17b) with respect to Y , we get

$$\begin{aligned} \frac{\partial u_1}{\partial X} &= \frac{Z^2 - H_1^2}{2} \frac{\partial^2 p_1}{\partial X^2} - H_1 X \frac{\partial p_1}{\partial X} + \frac{1}{2}(\beta_{10}^{r1}t_{13} - \beta_{10}^{r2}t_{23}) \\ &\quad + \frac{Z}{(2 + X^2 + Y^2)^2} \left[-(\beta_{10}^{r1}t_{13} + \beta_{10}^{r2}t_{23})(-2 + X^2) \right. \\ &\quad \left. + 2(-\gamma_{10}^{r1}t_{13} + \gamma_{10}^{r2}t_{23})XY + Y^2(\beta_{10}^{r1}t_{13} + \beta_{10}^{r2}t_{23}) \right], \end{aligned} \quad (\text{A18a})$$

$$\begin{aligned} \frac{\partial v_1}{\partial Y} &= \frac{Z^2 - H_1^2}{2} \frac{\partial^2 p_1}{\partial Y^2} - H_1 Y \frac{\partial p_1}{\partial Y} + \frac{1}{2}(\beta_{10}^{r1}t_{13} - \beta_{10}^{r2}t_{23}) \\ &\quad + \frac{Z}{(2 + X^2 + Y^2)^2} \left[(\beta_{10}^{r1}t_{13} + \beta_{10}^{r2}t_{23})(2 + X^2) \right. \\ &\quad \left. + 2(\gamma_{10}^{r1}t_{13} - \gamma_{10}^{r2}t_{23})XY - Y^2(\beta_{10}^{r1}t_{13} + \beta_{10}^{r2}t_{23}) \right]. \end{aligned} \quad (\text{A18b})$$

Adding Eqs. (A18a) and (A18b) we get

$$\begin{aligned} \frac{\partial u_1}{\partial X} + \frac{\partial v_1}{\partial Y} &= \frac{Z^2 - H_1^2}{2} \nabla^2 p_1 - H_1(\boldsymbol{\rho} \cdot \nabla)p_1 \\ &\quad + B + \frac{4Z}{(2 + X^2 + Y^2)^2} D_1, \end{aligned} \quad (\text{A19})$$

where $B = \beta_{10}^{r1}t_{13} - \beta_{10}^{r2}t_{23}$ and $D_1 = \beta_{10}^{r1}t_{13} + \beta_{10}^{r2}t_{23}$. Integrating Eq. (A19) with respect to Z between the two surfaces, and using the incompressibility condition, we get

$$\begin{aligned} \int_{H_1}^{H_2} \left(\frac{\partial u_1}{\partial X} + \frac{\partial v_1}{\partial Y} \right) dZ &= - \int_{H_1}^{H_2} \frac{\partial w_1}{\partial Z} dZ, \quad (\text{A20}) \\ \frac{2H_1^3}{3} \nabla^2 p_1 + 2H_1^2(\boldsymbol{\rho} \cdot \nabla)p_1 - 2BH_1 \\ &= \rho(\mathbf{E}_{12} \cdot \mathbf{e}_\rho + \mathbf{E}'_{12} \cdot \mathbf{e}_\phi), \end{aligned} \quad (\text{A21})$$

where $\mathbf{E}_{12} = \beta_{10}^{r1}\mathbf{t}_1 + \beta_{10}^{r2}\mathbf{t}_2$ and $\mathbf{E}'_{12} = \gamma_{10}^{r1}\mathbf{t}_1 - \gamma_{10}^{r2}\mathbf{t}_2$. Using the operators ∇^2 and ∇ in a cylindrical coordinate system, the above equation can be simplified as

$$\begin{aligned} \frac{2H_1^3}{3} \left[\frac{1}{\rho} \frac{\partial}{\partial \rho} \left(\rho \frac{\partial}{\partial \rho} \right) + \frac{1}{\rho^2} \frac{\partial^2}{\partial \phi^2} \right] p_1 + 2H_1^2 \rho \frac{\partial p_1}{\partial \rho} - 2BH_1 \\ = \rho(\mathbf{E}_{12} \cdot \mathbf{e}_\rho + \mathbf{E}'_{12} \cdot \mathbf{e}_\phi). \end{aligned} \quad (\text{A22})$$

Note that the pressure term does not contain a Z component. Let

$$p_1 = p_a + p_s(\mathbf{E}_{12} \cdot \mathbf{e}_\rho) + p_m(\mathbf{E}'_{12} \cdot \mathbf{e}_\phi), \quad (\text{A23})$$

where p_a , p_s , and p_m are the solutions of Eq. (A22). Inserting Eq. (A23) into Eq. (A22) we get the equation for the particular solution as

$$\frac{H_1^2}{3\rho} \frac{\partial}{\partial \rho} \left(\rho \frac{\partial p_a}{\partial \rho} \right) + H_1 \rho \frac{\partial p_a}{\partial \rho} - B = 0. \quad (\text{A24})$$

This gives us

$$p_a(\rho) = -B \left[\frac{3}{4H_1} + \frac{3}{8H_1^2} \right]. \quad (\text{A25})$$

Note that p_a has no ϕ dependency. The second term in Eq. (A23) (p_s) gives us

$$\begin{aligned} & \frac{2H_1^3}{3} \left[\frac{1}{\rho} \frac{\partial}{\partial \rho} \left(\rho \frac{\partial}{\partial \rho} \right) + \frac{1}{\rho^2} \frac{\partial^2}{\partial \phi^2} \right] p_s(\mathbf{E}_{12} \cdot \mathbf{e}_\rho) \\ & + 2H_1^2 \rho \frac{\partial}{\partial \rho} p_s(\mathbf{E}_{12} \cdot \mathbf{e}_\rho) = \rho(\mathbf{E}_{12} \cdot \mathbf{e}_\rho). \end{aligned} \quad (\text{A26})$$

Using the relations $\partial \mathbf{e}_\rho / \partial \rho = 0$, $\mathbf{e}_\phi = \partial \mathbf{e}_\rho / \partial \phi$, and $\mathbf{e}_\rho = -\partial \mathbf{e}_\phi / \partial \phi$, Eq. (A26) can be simplified as

$$\frac{2H_1^3}{3\rho} \frac{\partial}{\partial \rho} \left(\rho \frac{\partial p_s}{\partial \rho} \right) - \frac{2H_1^3}{3\rho^2} p_s + 2H_1^2 \rho \frac{\partial p_s}{\partial \rho} - \rho = 0. \quad (\text{A27})$$

The solution of Eq. (A27) is given by

$$p_s(\rho) = -\frac{6\rho}{5(2 + \rho^2)^2}. \quad (\text{A28})$$

One can follow a similar procedure to obtain the solution for $p_m(\rho)$ as

$$p_m(\rho) = -\frac{6\rho}{5(2 + \rho^2)^2}. \quad (\text{A29})$$

Incidentally, the solutions of p_s and p_m are the same. Therefore, from Eqs. (A25), (A28), and (A29) we get the solution for p_1 as

$$\begin{aligned} p_1 = & -B \left[\frac{3}{4H_1} + \frac{3}{8H_1^2} \right] - \frac{6\rho}{5(2 + \rho^2)^2} \\ & \times [(\beta_{10}^r \mathbf{t}_1 + \beta_{10}^r \mathbf{t}_2) \cdot \mathbf{e}_\rho + (\gamma_{10}^r \mathbf{t}_1 - \gamma_{10}^r \mathbf{t}_2) \cdot \mathbf{e}_\phi]. \end{aligned} \quad (\text{A30})$$

The corresponding velocity field [Eqs. (A17a) and (A17b)] of swimmer one can be determined in the lubrication region as

$$\begin{aligned} u_{\rho,1} = & \frac{3(Z^2 - H_1^2)}{10(2 + \rho^2)^3} [5B\rho^3 + 20B\rho - 4(\mathbf{e}_\rho \cdot \mathbf{E}_{12} + \mathbf{e}_\phi \cdot \mathbf{E}'_{12}) \\ & + 6\rho^2(\mathbf{e}_\rho \cdot \mathbf{E}_{12} + \mathbf{e}_\phi \cdot \mathbf{E}'_{12})] \\ & + \frac{Z\rho}{2H_1} D_1 + \frac{\rho}{2} B, \end{aligned} \quad (\text{A31a})$$

$$\begin{aligned} u_{\phi,1} = & \frac{6(Z^2 - H_1^2)}{10(2 + \rho^2)^2} [-\mathbf{e}_\phi \cdot \mathbf{E}_{12} + \mathbf{e}_\rho \cdot \mathbf{E}'_{12}] \\ & + \frac{Z\rho}{2H_1} [\gamma_{10}^r t_{23} - \gamma_{10}^r t_{13}] \\ & - \frac{\rho}{2} [\gamma_{10}^r t_{23} + \gamma_{10}^r t_{13}], \end{aligned} \quad (\text{A31b})$$

$$\begin{aligned} u_{z,1} = & \frac{Z}{20(2 + \rho^2)^4} [-5B(2 + \rho^2)^2 - 4Z^2] \\ & \times (-8 + 4\rho^2 + \rho^4) + 12(2 + \rho^2)^2(6 + \rho^2) \\ & \times (X(A_1 + C_2) + Y(-A_2 + C_1)) - 40D_1Z(2 + \rho^2)^2 \\ & + 32(-4 + \rho^2)(X(A_1 + C_2) + (-A_2 + C_1)Y)Z^2 \\ & + \frac{1}{2} [D_1 + X(-\beta_{10}^r t_{21} + \gamma_{10}^r t_{12} + \gamma_{10}^r t_{22}) \\ & - Y(\beta_{10}^r t_{22} + \gamma_{10}^r t_{11} + \gamma_{10}^r t_{21}) + \beta_{10}^r (t_{11}X + t_{12}Y)], \end{aligned} \quad (\text{A31c})$$

where $B = (\beta_{10}^r t_{13} - \beta_{10}^r t_{23})$, $D_1 = (\beta_{10}^r t_{13} + \beta_{10}^r t_{23})$, $A_1 = (\beta_{10}^r t_{11} + \beta_{10}^r t_{21})$, $C_1 = (\beta_{10}^r t_{12} + \beta_{10}^r t_{22})$, $A_2 = (\gamma_{10}^r t_{11} - \gamma_{10}^r t_{21})$, and $C_2 = (\gamma_{10}^r t_{12} - \gamma_{10}^r t_{22})$.

Finally, the force component along the Z direction can be calculated using the relation $dF_z = \mathbf{e}_z \cdot (\sigma_1 \cdot \mathbf{n}_1) dA$, where σ_1 is the corresponding stress tensor, dA is the area element on the swimmer surface, and $\mathbf{n}_1 = -\cos \theta \mathbf{e}_z + \sin \theta \mathbf{e}_\rho$ (normal vector; see Fig. 3). Subsequently, we can calculate the force component as

$$F_z = -\frac{3\pi Ba^2}{2} [-\ln(2) + \ln(2 + \rho_0^2)]. \quad (\text{A32})$$

Here, ρ_0 is the distance up to which the lubrication force is considerable. Generally, $\rho_0 = a\epsilon^{-1}$. Therefore,

$$F_z \approx \frac{3\pi Ba^2}{2} \ln \epsilon. \quad (\text{A33})$$

The corresponding torque along the Y direction can be calculated using the relation $dT_y = -(\mathbf{n}_1 \cdot \mathbf{e}_x) dF_z + (\mathbf{n}_1 \cdot \mathbf{e}_z) dF_x$. The torque is given by

$$\begin{aligned} T_y = & \epsilon^{1/2} \frac{3\pi}{10} [(\beta_{10}^r t_{11} + \beta_{10}^r t_{21}) + (\gamma_{10}^r t_{11} - \gamma_{10}^r t_{21})] \\ & \times \left[\frac{8}{2 + \rho^2} + 3 \ln(2 + \rho^2) + 4 + \ln 8 \right]. \end{aligned} \quad (\text{A34})$$

A similar expression for torque can be obtained about the X direction as well. However, note that torques are of the order $\epsilon^{1/2}$, and the contribution of the torques to the rotational motion of the swimmers is negligible. Thus, we do not include them in the numerical simulations.

APPENDIX B: χ - χ AND λ - λ STATE DIAGRAMS

As previously mentioned, a pair of chiral swimmers exhibits mainly B, D, and MD states in the presence of the lubrication forces. Figure 5 depicted these states for the choice $\lambda_1 = \lambda_2 = \lambda$ and $\chi_1 = \chi_2 = \chi$. However, one can also vary the parameters λ_1 , λ_2 , χ_1 , and χ_2 to study the hydrodynamic behavior of two chiral swimmers (see Fig. 9). With varying λ_1 , λ_2 , χ_1 , and χ_2 , swimmers mainly exhibit the D and MD states. Only the asymmetric combination of pusher- and puller-type swimmers exhibit bounded states for $|\lambda_1| = |\lambda_2|$ or $\chi_1 = \chi_2$. This means swimmers with the same \mathbf{V} and $\mathbf{\Omega}$, and equal strength of flow field (however, the sign of λ should be different) exhibit interesting bounded states. Note that when the swimmers are very close to each other, due to the lubrication force, swimmers

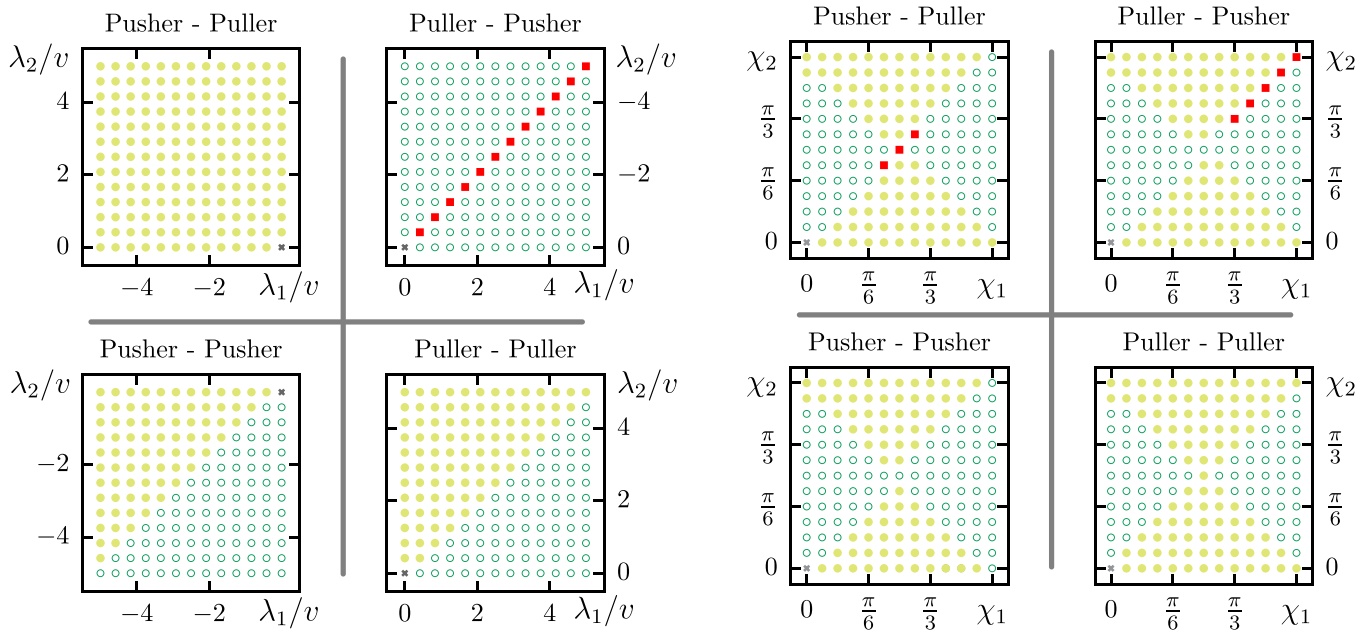


FIG. 9. State diagrams generated for varying hydrodynamic field strengths (λ_1, λ_2) at fixed $\chi_1 = \chi_2 = \chi$, and (χ_1, χ_2) at fixed $\lambda_1 = \lambda_2 = \lambda$. Initial conditions and color codes are given in Fig. 5.

repel each other strongly, and they do not exhibit either convergence (C) or monotonic convergence (MC) states. Sim-

ilar behavior can be observed in the case of axisymmetric squirmers.

- [1] E. M. Purcell, *Am. J. Phys.* **45**, 3 (1977).
- [2] J. Happel and H. Brenner, *Low Reynolds Number Hydrodynamics* (Springer, New York, 1983).
- [3] S. H. Larsen, R. Macnab, and D. E. Koshland, *Nature (London)* **249**, 74 (1974).
- [4] M. J. Lighthill, *Commun. Pure Appl. Math.* **5**, 109 (1952).
- [5] J. R. Blake, *J. Fluid Mech.* **46**, 199 (1971).
- [6] B. M. Friedrich and F. Jülicher, *Proc. Natl. Acad. Sci. USA* **104**, 13256 (2007).
- [7] E. M. Purcell, *Proc. Natl. Acad. Sci. USA* **94**, 11307 (1997).
- [8] H. R. Jiang, N. Yoshinaga, and M. Sano, *Phys. Rev. Lett.* **105**, 268302 (2010).
- [9] E. Lauga, *The Fluid Dynamics of Cell Motility* (Cambridge University Press, Cambridge, 2020).
- [10] J. R. Platt, *Science* **133**, 1766 (1961).
- [11] D. L. Kirchman, *Microb. Ecol.* **28**, 255 (1994).
- [12] J. Dunkel, S. Heidenreich, K. Drescher, H. H. Wensink, M. Bar, and R. E. Goldstein, *Phys. Rev. Lett.* **110**, 228102 (2013).
- [13] A. Sokolov and I. S. Aranson, *Phys. Rev. Lett.* **103**, 148101 (2009).
- [14] B. M. Haines, A. Sokolov, I. S. Aranson, L. Berlyand, and D. A. Karpeev, *Phys. Rev. E* **80**, 041922 (2009).
- [15] M. J. R. Fasham, H. W. Ducklow, and S. M. McKelvie, *J. Marine Res.* **48**, 591 (1990).
- [16] T. J. Pedley and J. O. Kessler, *Annu. Rev. Fluid Mech.* **24**, 313 (1992).
- [17] A. M. Metcalfe and T. J. Pedley, *J. Fluid Mech.* **445**, 121 (2001).
- [18] D. Saintillan and M. J. Shelley, *Phys. Rev. Lett.* **100**, 178103 (2008).
- [19] T. Ishikawa and M. Hota, *J. Exp. Biol.* **209**, 4452 (2006).
- [20] K. Drescher, K. C. Leptos, I. Tuval, T. Ishikawa, T. J. Pedley, and R. E. Goldstein, *Phys. Rev. Lett.* **102**, 168101 (2009).
- [21] T. J. Pedley, D. R. Brumley, and R. E. Goldstein, *J. Fluid Mech.* **798**, 165 (2016).
- [22] T. Ishikawa, T. J. Pedley, K. Drescher, and R. E. Goldstein, *J. Fluid Mech.* **903**, A11 (2020).
- [23] N. Darnton, L. Turner, K. Breuer, and H. C. Berg, *Biophys. J.* **86**, 1863 (2004).
- [24] T. Ishikawa, M. P. Simmonds, and T. J. Pedley, *J. Fluid Mech.* **568**, 119 (2006).
- [25] T. Ishikawa and T. J. Pedley, *Phys. Rev. Lett.* **100**, 088103 (2008).
- [26] I. O. Götze and G. Gompper, *Phys. Rev. E* **82**, 041921 (2010).
- [27] C. M. Pooley, G. P. Alexander, and J. M. Yeomans, *Phys. Rev. Lett.* **99**, 228103 (2007).
- [28] J. J. Molina, Y. Nakayama, and R. Yamamoto, *Soft Matter* **9**, 4923 (2013).
- [29] P. S. Burada, R. Maity, and F. Jülicher, *Phys. Rev. E* **105**, 024603 (2022).
- [30] H. C. Crenshaw, *Bull. Math. Biol.* **55**, 231 (1993).
- [31] O. S. Pak and E. Lauga, *J. Eng. Math.* **88**, 1 (2014).
- [32] S. Ghose and R. Adhikari, *Phys. Rev. Lett.* **112**, 118102 (2014).
- [33] B. U. Felderhof and R. B. Jones, *Phys. Fluids* **28**, 073601 (2016).
- [34] B. U. Felderhof, [arXiv:1601.00755](https://arxiv.org/abs/1601.00755).

- [35] R. Maity and P. S. Burada, *Eur. Phys. J. E* **42**, 20 (2019).
- [36] R. Maity and P. S. Burada, *J. Fluid Mech.* **940**, A13 (2022).
- [37] M. Mirzakhloo, M. A. Jalali, and M. R. Alam, *Sci. Rep.* **8**, 3670 (2018).
- [38] M. Theers, E. Westphal, G. Gompper, and R. G. Winkler, *Soft Matter* **12**, 7372 (2016).
- [39] H. A. Stone and A. D. T. Samuel, *Phys. Rev. Lett.* **77**, 4102 (1996).
- [40] S. Kim and S. J. Karrila, *Microhydrodynamics: Principles and Selected Applications* (Dover, New York, 1991).
- [41] R. Di Leonardo, L. Angelani, D. Dell'Arciprete, G. Ruocco, V. Iebba, S. Schippa, M. P. Conte, F. Mecarini, F. De Angelis, and E. Di Fabrizio, *Proc. Natl. Acad. Sci.* **107**(21), 9541 (2010).
- [42] R. Trouilloud, T. S. Yu, A. E. Hosoi, and E. Lauga, *Phys. Rev. Lett.* **101**, 048102 (2008).
- [43] S. Wang and A. M. Ardekani, *Phys. Rev. E* **87**, 063010 (2013).
- [44] R. Di Leonardo, D. Dell'Arciprete, L. Angelani, and V. Iebba, *Phys. Rev. Lett.* **106**, 038101 (2011).
- [45] N. Yoshinaga and T. B. Liverpool, *Phys. Rev. E* **96**, 020603(R) (2017).
- [46] W. F. Paxton, K. C. Kistler, C. C. Olmeda, A. Sen, S. K. St. Angelo, Y. Cao, T. E. Mallouk, P. E. Lammert, and V. H. Crespi, *J. Am. Chem. Soc.* **126**, 13424 (2004).
- [47] R. F. Ismagilov, A. Schwartz, N. Bowden, and G. M. Whitesides, *Angew. Chem., Int. Ed.* **41**, 652 (2002).
- [48] R. Golestanian, T. B. Liverpool, and A. Ajdari, *Phys. Rev. Lett.* **94**, 220801 (2005).
- [49] R. Dreyfus, J. Baudry, M. L. Roper, M. Fermigier, H. A. Stone, and J. Bibette, *Nature (London)* **437**, 862 (2005).
- [50] T. Hogg, *Auton. Agents Multi-Agent Syst.* **14**, 271 (2007).